NASA Technical Memorandum 103911

# Computation of Incompressible Viscous Flows through Turbopump Components

Cetin Kiris, Dochan Kwak, and Stuart Rogers



March 1992

National Aeronautics and Space Administration

NASA Technical Memorandum 103911

# Computation of Incompressible Viscous Flows through Turbopump Components

Cetin Kiris, MCAT Institute, Moffett Field, California
Dochan Kwak and Stuart Rogers, Ames Research Center, Moffett Field, California

March 1992

National Aeronautics and
Space Administration

**Ames Research Center**
Moffett Field, California 94035-1000

# COMPUTATION OF INCOMPRESSIBLE VISCOUS FLOWS THROUGH TURBOPUMP COMPONENTS



Cetin Kiris,* Dochan Kwak, and Stuart Rogers

Ames Research Center

## SUMMARY

A finite-difference, three-dimensional, incompressible Navier-Stokes formulation for calculating the flow through turbopump components is presented. The solution method is based on the pseudocompressibility approach and uses an implicit-upwind differencing scheme together with the Gauss-Seidel line-relaxation method. Both steady and unsteady flow calculations can be performed using the presented algorithm. In this paper, the equations are solved in steadily rotating reference frames by using the steady-state formulation in order to simulate the flow through a turbopump inducer. Eddy viscosity is computed by using the Baldwin-Lomax model. Numerical results are compared with experimental measurements and good agreement is found between the two. Time-accurate calculations will be reported in future publications.

## INTRODUCTION

With the advent of supercomputer hardware, as well as fast numerical methods, computational fluid dynamics (CFD) has become an essential part of aerospace research and design. Numerical studies in incompressible flows show good progress in parallel with computational studies in compressible flows. For example, the incompressible flow solver developed by Kwak et al. (ref. 1) was extensively used for simulating the flow through the main engine power-head components of the space shuttle. The redesign of the main engine hot-gas manifold of the space shuttle, guided by the computations of Chang et al. (ref. 2), illustrates the usefulness of CFD in aerospace research. Since the incompressible Navier-Stokes formulation does not yield the pressure field explicitly from the equation of state or through the continuity equation, numerical solution of the equations requires special attention in order to satisfy the divergence-free constraint on the velocity field.

The most widely used methods that use primitive variables are the fractional-step and pseudocompressibility techniques. In the fractional-step method, the auxiliary velocity field is solved by using the momentum equations. A Poisson equation for pressure is then formed by taking the divergence of the momentum equations and by using a divergence-free velocity-field constraint. Solving the Poisson equation for pressure efficiently in three-dimensional curvilinear coordinates is the most important feature

* MCAT Institute, Moffett Field, California.

of the fractional-step method (ref. 3). One way to avoid the numerical difficulty imposed by the elliptic nature of the problem is to use the pseudocompressibility method. With the pseudocompressibility method, the elliptic-parabolic-type equations are transformed into hyperbolic-parabolic-type equations. Well-established solution algorithms developed for compressible flows can be utilized to solve the resulting equations.

Steger and Kutler (ref. 4) employed an alternating-direction implicit scheme in Chorin's (ref. 5) pseudocompressibility method. This formulation was extended to three-dimensional generalized coordinates by Kwak et al. (ref. 1). Recently, a three-dimensional incompressible Navier-Stokes solver (INS3D-LU-SGS) using a lower-upper-symmetric Gauss-Seidel algorithm was developed by Yoon and Kwak (ref. 6). This algorithm is used to calculate the inducer flow of the main-engine turbopump of the space shuttle in order to demonstrate the performance of the numerical method (ref. 7). Another effort is reported in reference 8 in which upwind differencing and the Gauss-Seidel line-relaxation scheme were used in order to have a robust and fast-converging scheme (INS3D-UP). A time-accurate formulation of this algorithm is implemented for incompressible flows through artificial heart devices with moving boundaries (refs. 8-10). In the present study, the steady-state formulation is used in steadily rotating reference frames in order to develop a CFD procedure for simulating the flow through the turbopump components of a liquid rocket engine.

In the first section, the governing equations and numerical method are described. Following that is a presentation of the computed results obtained from the current approach.

The authors would like to thank Mr. Liang-Pang Chang of MCAT Institute for providing grid-generation and graphical support for this study. This work is partially supported by the NASA Marshall Space Flight Center. Computer time was provided by the Numerical Aerodynamic Simulation (NAS) facility at Ames Research Center.

## GOVERNING EQUATIONS AND METHOD OF SOLUTION

The algorithm used in both steady and unsteady formulations is based on the method of pseudocompressibility, which produces a hyperbolic system of equations by introducing a time-derivative pressure term into the continuity equation. The resulting incompressible Navier-Stokes equations can be written in a generalized curvilinear coordinate system $(\xi, \eta, \zeta)$ as follows:

$$\frac{\partial Q}{\partial \tau} + \frac{\partial}{\partial \xi}(E - E_v) + \frac{\partial}{\partial \eta}(F - F_v) + \frac{\partial}{\partial \zeta}(G - G_v) = S \tag{1}$$

where $Q$, and the convective flux vectors $E$, $F$, $G$, are

$$Q = \frac{1}{J}\begin{bmatrix} p \\ u \\ v \\ w \end{bmatrix}$$

$$E = \frac{1}{J}\begin{bmatrix} \beta U \\ \xi_x p + uU + \xi_t u \\ \xi_y p + vU + \xi_t v \\ \xi_z p + wU + \xi_t w \end{bmatrix}$$

$$F = \frac{1}{J}\begin{bmatrix} \beta V \\ \eta_x p + uV + \eta_t u \\ \eta_y p + vV + \eta_t v \\ \eta_z p + wV + \eta_t w \end{bmatrix}$$

$$G = \frac{1}{J}\begin{bmatrix} \beta W \\ \zeta_x p + uW + \zeta_t u \\ \zeta_y p + vW + \zeta_t v \\ \zeta_z p + wW + \zeta_t w \end{bmatrix}$$

Here $J$, $\beta$, $p$, $u$, $v$, and $w$ denote the Jacobian of transformation, the pseudocompressibility coefficient, pressure, and Cartesian velocity components, respectively. The contravariant velocity components $U$, $V$, and $W$ are defined as

$$U = \xi_x u + \xi_y v + \xi_z w$$
$$V = \eta_x u + \eta_y v + \eta_z w$$
$$W = \zeta_x u + \zeta_y v + \zeta_z w$$

For an orthogonal-grid assumption, the viscous flux vectors $E_v$, $F_v$, and $G_v$ are given by

$$E_v = \frac{1}{ReJ}\begin{bmatrix} (\xi_x^2 + \xi_y^2 + \xi_z^2)u_\xi \\ (\xi_x^2 + \xi_y^2 + \xi_z^2)v_\xi \\ (\xi_x^2 + \xi_y^2 + \xi_z^2)w_\xi \end{bmatrix}$$

$$F_v = \frac{1}{ReJ}\begin{bmatrix} (\eta_x^2 + \eta_y^2 + \eta_z^2)u_\eta \\ (\eta_x^2 + \eta_y^2 + \eta_z^2)v_\eta \\ (\eta_x^2 + \eta_y^2 + \eta_z^2)w_\eta \end{bmatrix}$$

$$G_v = \frac{1}{ReJ}\begin{bmatrix} (\zeta_x^2 + \zeta_y^2 + \zeta_z^2)u_\zeta \\ (\zeta_x^2 + \zeta_y^2 + \zeta_z^2)v_\zeta \\ (\zeta_x^2 + \zeta_y^2 + \zeta_z^2)w_\zeta \end{bmatrix}$$

where $Re$ is the Reynolds number. For simplicity, the viscous terms are written for the orthogonal grid and the constant viscosity case. However, the algorithm includes the terms necessary for a nonorthogonal-grid case and for a nonconstant-viscosity case. When the equations are solved in steadily rotating reference frames, the centrifugal force and the Coriolis force are added to the equations of motion as source terms. In this case, the equations are written for relative velocity components in a moving relative frame of reference. The source term $S$ is given by

$$S = \begin{bmatrix} 0 \\ 0 \\ \Omega(\Omega y + 2w) \\ \Omega(\Omega z - 2v) \end{bmatrix}$$

where $\Omega$ is the rotational speed. Relative velocity components are written in terms of

absolute velocity components $u_a$, $v_a$, and $w_a$ as

$$u = u_a$$
$$v = v_a + \Omega z$$
$$w = w_a - \Omega y$$

In other cases, the source term $S$ is set to zero. In the steady-state formulation, the time-derivatives are differenced by using the Euler backward formula. The equations are solved iteratively in pseudotime until the the solution converges to a steady state. In the time-accurate formulation, the time-derivatives in the momentum equations are differenced by using a second-order, three-point, backward-difference formula. The equations are iterated to convergence in pseudotime for each physical time-step until a divergence-free velocity field is obtained. Central differencing is used to numerically compute the viscous flux derivatives, because they have well-behaved diffusive terms. However, higher-order upwind differencing is employed to compute the convective flux derivatives. The reason for using an upwind scheme is to have a more reliable, robust, and general-purpose solution algorithm. Chakravarthy and Osher outline the class of high-accuracy flux differencing schemes for compressible flow equations (ref. 11). Following the third-order scheme of reference 11, a fifth-order-accurate, upwind-biased stencil is derived by Rai (ref. 12). The upwind differencing used here is the implementation of those efforts on incompressible Navier-Stokes equations. The $\xi$-derivative of the convective flux $E$ can be written as

$$\frac{\partial E}{\partial \xi} \approx \frac{[E_{i+1/2} - E_{i-1/2}]}{\Delta \xi}$$

The numerical flux $E_{i+1/2}$ is defined as follows:

$$E_{i+1/2} = \frac{1}{2}\left[E(Q_{i+1}) + E(Q_i) - \phi_{i+1/2}\right] \tag{2}$$

where the $\phi_{i+1/2}$ is a dissipation term. The order of the scheme is determined by the definition of the dissipation term $\phi_{i+1/2}$. For $\phi_{i+1/2} = 0$, the differencing is reduced to a second-order central-difference scheme. A first-order upwind flux is defined by

$$\phi_{i+1/2} = \left(\Delta E^+_{i+1/2} - \Delta E^-_{i+1/2}\right) \tag{3}$$

and a third-order upwind flux is given by

$$\phi_{i+1/2} = -\frac{1}{3}\left(\Delta E^+_{i-1/2} - \Delta E^+_{i+1/2} + \Delta E^-_{i+1/2} - \Delta E^-_{i+3/2}\right) \tag{4}$$

Finally, the following dissipation term creates a fifth-order upwind-biased scheme that requires seven stencil points:

$$\begin{aligned}\phi_{i+1/2} = &-\frac{1}{30}(-2\Delta E^+_{i-3/2} + 11\Delta E^+_{i-1/2} - 6\Delta E^+_{i+1/2} - 3\Delta E^+_{i+3/2} + 2\Delta E^-_{i+5/2} \\ &- 11\Delta E^-_{i+3/2} + 6\Delta E^-_{i+1/2} + 3\Delta E^-_{i-1/2})\end{aligned} \tag{5}$$

where $\Delta E^{\pm}$ is the flux difference across positive or negative traveling waves, and is

computed as

$$\Delta E^{\pm}_{i+1/2} = A^{\pm}(\bar{Q})\Delta Q_{i+1/2}$$

Here, $A^{\pm}$ is the plus (minus) Jacobian matrix. The $\Delta$ operator, and $\bar{Q}$ are given by

$$\Delta Q_{i+1/2} = Q_{i+1} - Q_i \ .$$

$$\bar{Q} = \frac{1}{2}(Q_{i+1} + Q_i)$$

A special treatment is neccesary next to the boundary when third- and fifth-order differencing schemes are used. The differencing near the boundary is

$$\frac{\partial E}{\partial \xi} \approx \frac{[E_{i=5/2} - E_{i=3/2}]}{\Delta \xi}$$

For the flux terms, both at $i = 3/2$ and at $i = 5/2$, the first-order terms are used. The differencing between the flux at $i = 7/2$ and the flux at $i = 5/2$ is increased to third-order differencing by using third-order flux terms at both points. This requires storing both first- and third-order flux terms at $i = 5/2$.

An implicit, delta-law-form approximation to equation (1) after linearization in time and the use of approximate Jacobians of the flux differences results in a seven-block diagonal matrix equation written as

$$\begin{aligned} \bar{B}\delta Q_{i-1,j,k} + \bar{A}\delta Q_{i,j,k} + \bar{C}\delta Q_{i+1,j,k} + \bar{D}\delta Q_{i,j-1,k} + \bar{E}\delta Q_{i,j+1,k} + \bar{F}\delta Q_{i,j,k-1} \\ + \bar{G}\delta Q_{i,j,k+1} = R.H.S. \end{aligned} \tag{6}$$

where $\delta Q = Q^{n+1} - Q^n$ and $\bar{A}, \bar{B}, \bar{C}, \bar{D}, \bar{E}, \bar{F}$, and $\bar{G}$ are 4 x 4 block diagonals.

The solution method of this matrix equation greatly affects the efficiency and the robustness of the whole algorithm. An approximate factorization (AF) scheme introduces a time-step limitation owing to factorization error (ref. 13). Since the flux-difference splitting requires more computer time than central differencing, using an unbounded time-step is important in order to reach the efficiency of a Newton procedure. The Gauss-Seidel line-relaxation scheme, which was succesfully employed by MacCormack (ref. 14), allows an unbounded time-step to be taken.

In equation (6), the right-hand-side term is computed and stored for the entire domain. The Gauss-Seidel line-relaxation procedure is composed of three stages, each of which involves a block-tridiagonal inversion in one direction. In the first stage, $\delta Q$ is solved line-by-line in one direction. Before the block-tridiagonal equation is solved, off-tridiagonal terms are multiplied by the current value of $\delta Q$ and are then shifted over to the right-hand side of the equation. In other words, equation (6) is solved by performing a block-tridiagonal inversion in the $\xi$-direction, and Gauss-Seidel sweeps in the $\eta$- and $\zeta$-directions. After the first sweep is completed for the entire domain, a second sweep is started in the opposite direction. One forward sweep and one backward sweep suffice for most of the problems, but the number of sweeps can be increased. The second stage is to solve the block-tridiagonal terms in the $\eta$-direction and to perform backward and forward sweeps in the $\zeta$- and $\xi$-directions. The same procedure is repeated in the third stage by inverting the block-tridiagonal matrix in the $\zeta$-direction and treating the off-line terms for the $\xi$- and $\eta$-directions in Gauss-Seidel fashion.

Implicit boundary conditions are used at all of the boundaries except at the zonal and overlapped interface boundaries; zonal and grid-embedding interface boundaries are explicitly updated. No-slip boundary conditions are imposed at the solid stationary wall where the velocities are zero. The pressure boundary condition is specified such that the pressure gradient normal to the wall is zero.

At the inflow and outflow boundaries, characteristic boundary conditions are employed implicitly. It is assumed that the effect of viscous terms at the boundaries is negligible. Also, the characteristic equations are approximated in one-dimensional space. The primitive variables that are needed at the boundaries are the pressure $p$ and the velocity components $u$, $v$, and $w$. The number of positive and negative eigenvalues of the Jacobian matrix of the convective flux determines how many variables should be specified at the boundaries. If the flow is in the positive $\xi$-direction then three of the eigenvalues are positive and one of them is negative. Therefore, there will be three characteristic waves traveling downstream and one characteric wave traveling upstream. In that case, the exit boundary receives information about the three variables by means of the characteristics traveling from the interior of the domain. Hence, only one variable should be specified at the outflow boundary. However, the inflow boundary is informed by only one characteristic traveling from the interior region. Therefore, three variables should be specified at the inflow boundary. Details of the numerical method are given in reference 8.

## COMPUTED RESULTS

The flow field through a turbopump inducer is solved as a benchmark problem in order to validate the CFD procedure for turbomachinery applications. In this section, results obtained for the Rocketdyne inducer shown in figure 1 are presented. The inducer geometry was developed and experimentally studied by the Rocketdyne Division of Rockwell International. The design flow is 2,236 gal/min with a design speed of 3,600 rpm. In the computational study, tip-leakage effects are included with a tip clearance of 0.008 inch. The problem was nondimensionalized with a tip diameter of 6.0 inches and an average inflow velocity of 28.3 ft/sec. The Reynolds number for this calculation was 191,800 per inch. The upstream section of the inducer was taken as a 2-tip-diameter-long straight channel, as shown in figure 1. The bull-nose of the inducer was treated as a rotating wall, and the cavity section was neglected. However, this region can be included by using an additional zone. An H-H grid topology with dimensions of 187 $\times$ 27 $\times$ 35 was used. A partial view of the surface grid is shown in figure 2. An H-type surface grid was generated for each surface using an elliptic grid generator. The interior region of the three-dimensional grid was filled using an algebraic solver coupled with an elliptic smoother. In the straight channel, the grid was generated for one-sixth of the cross section of the tube. This grid was extended to the outflow section of the inducer between the blades. Periodic boundary conditions were used at the endpoints in the rotational direction.

At the inflow and outflow boundaries, characteristic boundary conditions were employed. At the inflow, $v$ and $w$ velocity components were specified as zero, and the total pressure was specified as constant. Axial velocity and static pressure were

calculated from the characteristic relation and the total pressure relation. At the outflow, static pressure was specified and the velocity components were computed from the characteristics propagating from the interior region. The flow was taken at rest initially and the inducer was fully rotated impulsively. The solution was considered converged when the maximum residual dropped at least four orders of magnitude. This was obtained in less than 500 iterations. The computer time required per grid point per iteration was about $1.4 \times 10^{-4}$ sec.

Figure 3 illustrates the planes where the experimental measurements were taken by Rocketdyne. Axial and tangential velocity components and the flow angle were measured in planes A, B, C, and D at various circular arcs from the hub to the tip region. At each plane, the comparison between experimental measurements and numerical results along three of the circular arcs is presented in this paper. A total velocity and a flow angle are compared with the experimental data. The total velocity has only a tangential and an axial velocity component. The radial velocity component was not measured in the experiment.

Figures 4 through 7 show relative total velocities and relative flow angles as a function of circumferential angle in planes A, B, C, and D, respectively. The circumferential angle increases from the suction side to the pressure side. The comparison of computed and experimental results is generally good all the way from the hub to tip region. The difference between the experimental data and the numerical results is about 5%-8% in velocity. In all planes, the hub and tip regions show the biggest discrepancies. This may be a result of the relatively coarse grid used for the boundary layer. In the computational study, the Baldwin-Lomax algebraic turbulence model is used to determine the eddy viscosity. The comparison shows that the solution algorithm does a good job with an algebraic turbulence model. Implementation of the one-equation model of Baldwin and Barth (ref. 15) is under way for the present algorithm.

The reason for higher-order turbulence modeling is the comparisons obtained in plane D, in which the wake region is not predicted accurately (fig. 7). Another advantage of the one-equation model is that there is no need to define a length-scale explicitly. Near the tip-clearance region, the difference between experimental measurements and numerical results is noticeably larger than the error in other regions. This is due to the lack of grid resolution in the tip-clearance region. In the grid-refinement study, the number of grid points in the tip-clearance region was increased from four to nine. In the coarse-grid computation there is one overlapped grid point in the rotational direction to ensure periodic boundary conditions. In the fine grid, three additional zones were added in radial direction. The results with the one-equation model and the results from the grid-refinement study will be published later.

Figure 8 shows the surface of the inducer color-coded by nondimensionalized pressure. The pressure gradients across the blades caused by the action of centrifugal force and the pressure rise from inflow to outflow are illustrated. This pressure rise along the inducer can also be seen in figure 9. Velocity vectors are plotted in the meridional plane and the vectors are colored by the static pressure. The existing solution procedure can be applied to the same configuration under off-design conditions. The massive separation, which may block the fuel supply, can be detected in the numerical study.

This separation will be the subject of our future work which is intended to produce a pre-design and post-design engineering tool in challenging turbomachinery applications.

## CONCLUDING REMARKS

An efficient and robust solution procedure was developed and validated for three-dimensional turbopump applications. Numerical simulations of the flow through a Rocketdyne inducer were successfully carried out by using CFD techniques for solving viscous incompressible Navier-Stokes equations with the source terms in steadily rotating reference frames. The method of pseudocompressibility with a higher-order accurate upwind differencing and the Gauss-Seidel line-relaxation scheme provide fast convergence and robustness. Results in the form of relative total velocity and relative flow angle in four planes are presented. Numerical results compare fairly well with experimental data.

## REFERENCES


1. Kwak, D.; Chang, J. L. C.; Shanks, S. P.; and Chakravarthy, S.: A Three-Dimensional Incompressible Navier-Stokes Flow Solver Using Primitive Variables. AIAA J., vol. 24, no. 3, 1977, pp. 390-396.
2. Chang, J. L. C.; Kwak, D.; Rogers, S. E.; and Yang, R.-J.: Numerical Simulation Methods of Incompressible Flows and an Application to the Space Shuttle Main Engine. Int. J. Num. Meth. Fluids, vol. 8, 1988, pp. 1241-1268.
3. Rosenfeld, M.; Kwak, D.; and Vinokur, M.: A Fractional Step Solution Method for the Unsteady Incompressible Navier-Stokes Equations in Generalized Coordinate Systems. Journal of Computational Physics, 1991, in press.
4. Steger, J. L.; and Kutler, P.: Implicit Finite-Difference Procedures for the Computation of Vortex Wakes. AIAA J., vol. 15, no. 4, Apr. 1977, pp. 581-590.
5. Chorin, A. J.: A Numerical Method for Solving Incompressible Viscous Flow Problems. J. Comput. Phys., vol. 2, 1967, pp. 12-26.
6. Yoon, S.; and Kwak, D.: Three-Dimensional Incompressible Navier-Stokes Solver Using Lower-Upper Symmetric-Gauss-Seidel Algorithm. AIAA J., vol. 29, no. 4, 1991, pp. 874-875.
7. Yoon, S.; and Kwak, D.: Implict Methods for the Navier-Stokes Equations. Comput. Sys. Eng., vol. 1, nos. 2-4, 1990, pp. 535-547.
8. Rogers, S. E.; Kwak, D.; and Kiris, C.: Numerical Solution of the Incompressible Navier-Stokes Equations for Steady and Time-Dependent Problems. AIAA J., vol. 29, no. 4, 1991, pp. 603-610.
9. Kiris, C.; Chang, I.; Rogers, S. E.; and Kwak, D.: Numerical Simulation of the the Incompressible Internal Flow through a Tilting Disk Valve. AIAA Paper 90-0682, 1990.
10. Kiris, C.; Rogers, S. E.; Kwak, D.; and Chang, I.: Computation of Incompressible Viscous Flows with Moving Boundaries. Proceedings of the International Symposium on Biofluiddynamics, Seattle, Wash., July 1991.
11. Chakravarthy, S. R.; and Osher, S.: A New Class of High Accuracy TVD Schemes for Hyperbolic Conservation Laws. AIAA Paper 85-0363, 1985.
12. Rai, M. M.: Unsteady Three-Dimensional Navier-Stokes Simulations of Turbine Rotor-Stator Interaction. AIAA Paper 87-2058, 1987.
13. Beam, R. M.; and Warming, R. F.: An Implicit Finite-Difference Algorithm for Hyperbolic Systems in Conservation-Law Form. J. Comput. Phys., vol. 22, 1976, pp. 87-109.
14. MacCormack, R. W.: Current Status of Numerical Solutions of the Navier-Stokes Equations. AIAA Paper 85-0032, 1985.
15. Baldwin, B. S.; and Barth, T. J.: A One-Equation Turbulence Transport Model for High Reynolds Number Wall-Bounded Flows. AIAA Paper 91-0610, 1991.

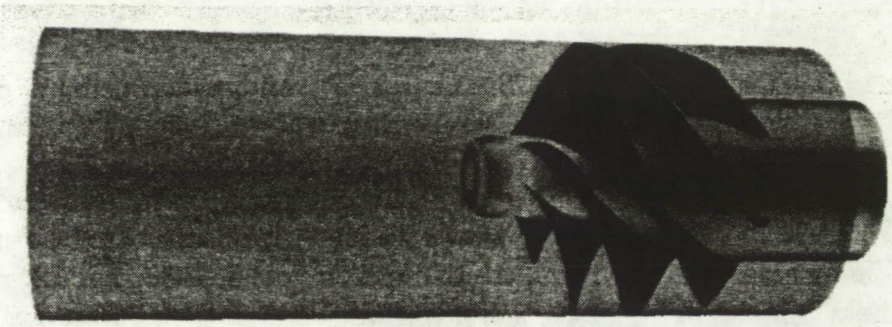

Figure 1. Rocketdyne turbopump inducer configuration.

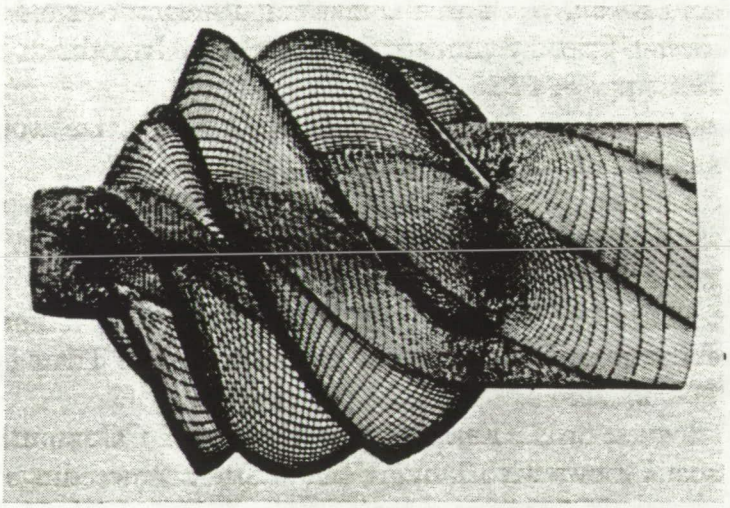

Figure 2. Surface grid for Rocketdyne turbopump inducer.

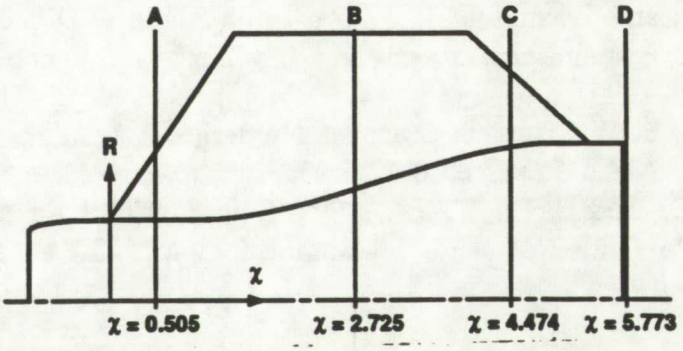


Figure 3. Schematic representation of planes where experimental data are available.

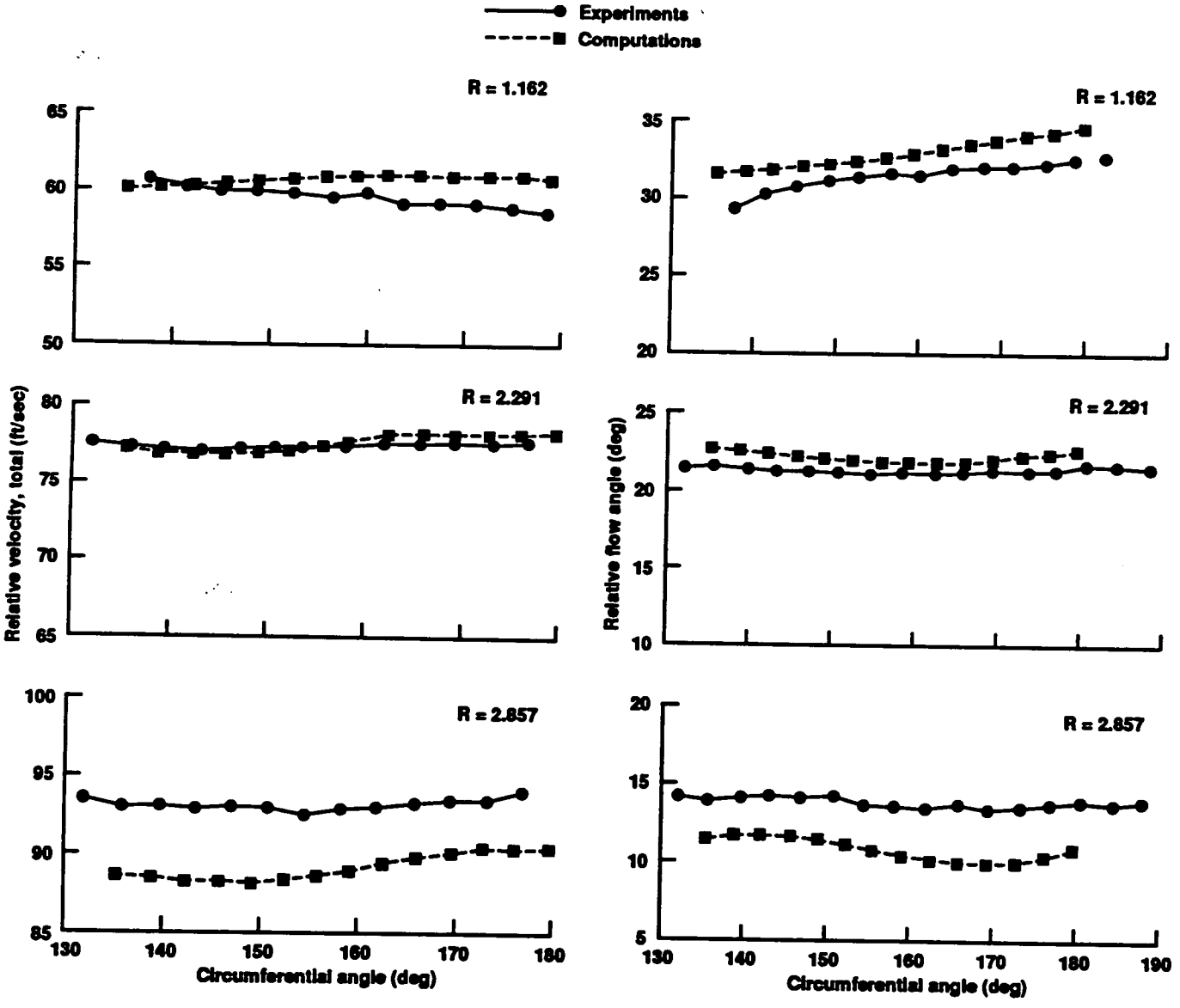


Figure 4. Comparison of relative total velocity and relative flow angle in plane A.

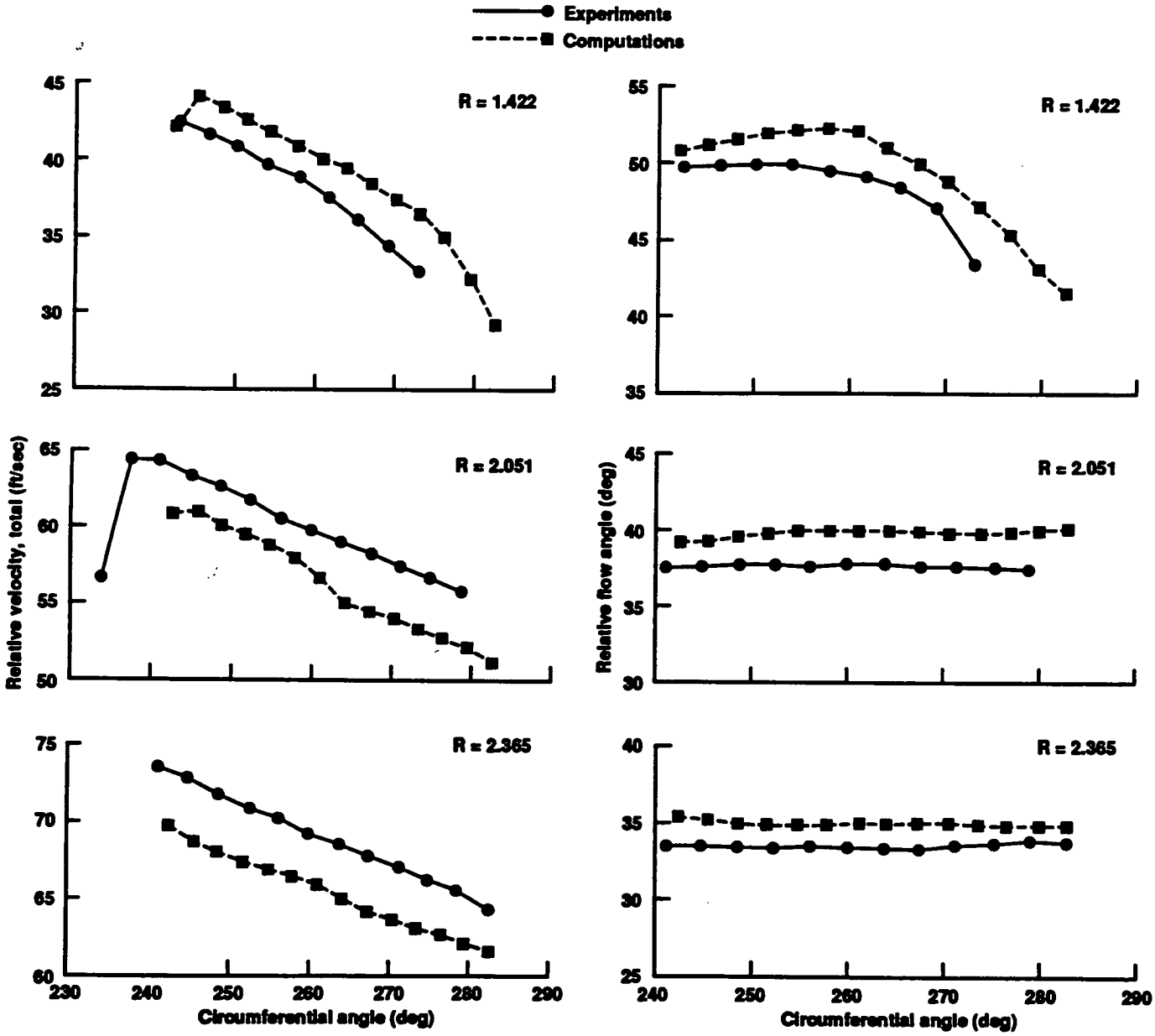


Figure 5. Comparison of relative total velocity and relative flow angle in plane B.

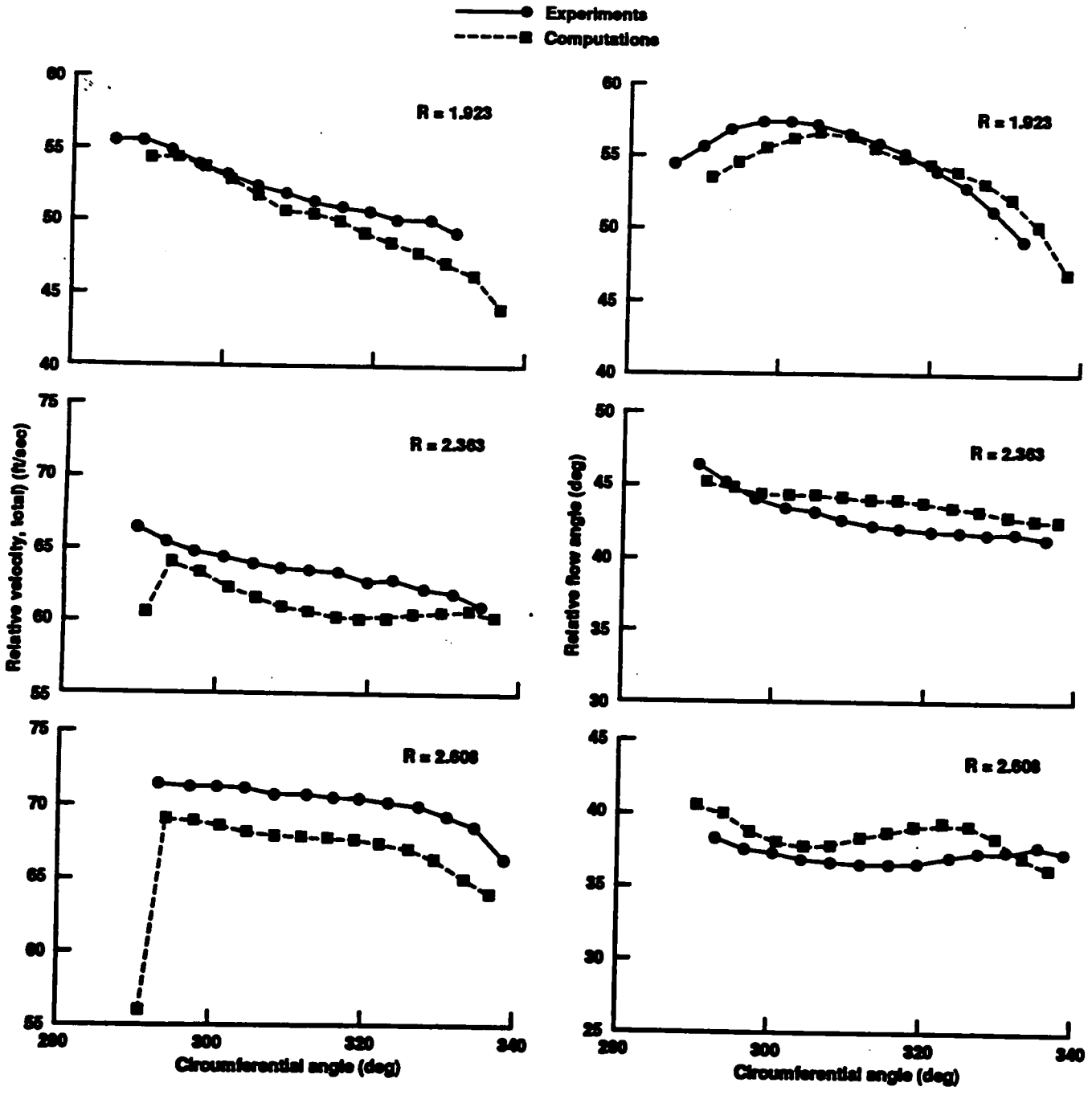


Figure 6. Comparison of relative total velocity and relative flow angle in plane C.

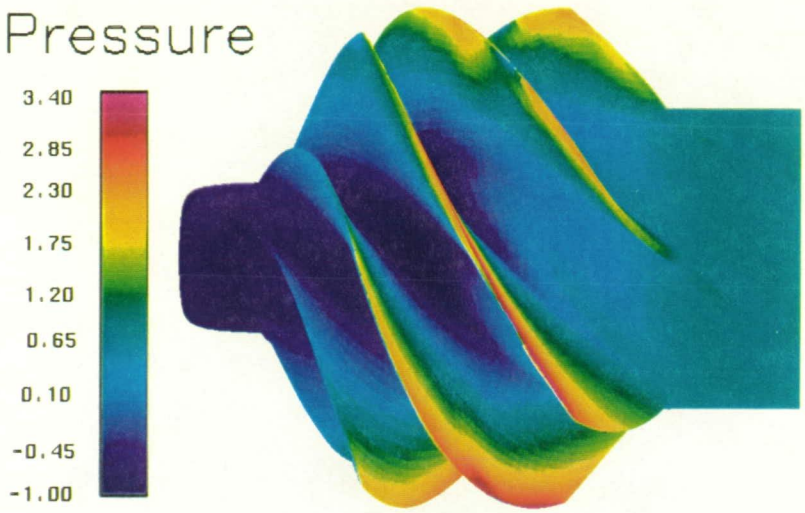


Figure 8. Surface pressure for Rocketdyne inducer.


Figure 9. Velocity vectors colored by pressure on the meridional plane of the inducer.

# REPORT DOCUMENTATION PAGE

Form Approved
OMB No. 0704-0188



| 1. AGENCY USE ONLY *(Leave blank)* | 2. REPORT DATE | 3. REPORT TYPE AND DATES COVERED |
|---|---|---|
| | March 1992 | Technical Memorandum |

**4. TITLE AND SUBTITLE**

Computation of Incompressible Viscous Flows through Turbopump Components

**5. FUNDING NUMBERS**

505-59

**6. AUTHOR(S)**

Cetin Kiris,* Dochan Kwak, and Stuart Rogers

**7. PERFORMING ORGANIZATION NAME(S) AND ADDRESS(ES)**

Ames Research Center
Moffett Field, CA 94035-1000

**8. PERFORMING ORGANIZATION REPORT NUMBER**

A-92041

**9. SPONSORING/MONITORING AGENCY NAME(S) AND ADDRESS(ES)**

National Aeronautics and Space Administration
Washington, DC 20546-0001

**10. SPONSORING/MONITORING AGENCY REPORT NUMBER**

NASA TM-103911

**11. SUPPLEMENTARY NOTES**

Point of Contact: Cetin Kiris, Ames Research Center, MS 258-1, Moffett Field, CA 94035-1000
(415) 604-4485 or FTS 464-4485
*MCAT Institute, Moffett Field, California

**12a. DISTRIBUTION/AVAILABILITY STATEMENT**

Unclassified — Unlimited
Subject Category 34

**12b. DISTRIBUTION CODE**

**13. ABSTRACT** *(Maximum 200 words)*

A finite-difference, three-dimensional, incompressible Navier-Stokes formulation for calculating the flow through turbopump components is presented. The solution method is based on the pseudocompressibility approach and uses an implicit-upwind differencing scheme together with the Gauss-Seidel line-relaxation method. Both steady and unsteady flow calculations can be performed using the presented algorithm. In this paper, the equations are solved in steadily rotating reference frames by using the steady-state formulation in order to simulate the flow through a turbopump inducer. Eddy viscosity is computed by using the Baldwin-Lomax model. Numerical results are compared with experimental measurements and good agreement is found between the two. Time-accurate calculations will be reported in future publications.

**14. SUBJECT TERMS**

Incompressible Navier-Stokes, Turbopump component, Implicit-upwind differencing

**15. NUMBER OF PAGES**

20

**16. PRICE CODE**

A02

| 17. SECURITY CLASSIFICATION OF REPORT | 18. SECURITY CLASSIFICATION OF THIS PAGE | 19. SECURITY CLASSIFICATION OF ABSTRACT | 20. LIMITATION OF ABSTRACT |
|---|---|---|---|
| Unclassified | Unclassified | | |